Received: 12 June 2019 | Revised: 4 August 2019 | Accepted: 4 August 2019

DOI: 10.1111/jace.16732

ORIGINAL ARTICLE

Journal of the American Ceramic Society

Viscosity and liquidus-based predictor of glass-forming ability of oxide glasses

Jeanini Jiusti | **Edgar D. Zanotto** | **Daniel R. Cassar** | **Marcello R. B. Andreeta**

Center of Research, Technology, and Education in Vitreous Materials (CeRTEV), Federal University of São Carlos (UFSCar), Graduate Program in Materials Science and Engineering, São Carlos, SP, Brazil

Correspondence
Jeanini Jiusti, Department of Materials Engineering (DEMa), Center of Research, Technology, and Education in Vitreous Materials (CeRTEV), Federal University of São Carlos (UFSCar), 13.565-905 São Carlos, SP, Brazil.
Email: jeaninijiusti@gmail.com

Funding information
Coordenação de Aperfeiçoamento de Pessoal de Nível Superior, Grant/Award Number: 001; Conselho Nacional de Desenvolvimento Científico e Tecnológico, Grant/Award Number: 141107/2016-2 and 300959/2010-9; Fundação de Amparo à Pesquisa do Estado de São Paulo, Grant/Award Number: 2013/07793-6 and 2017/12491-0

Abstract

Glass-forming ability (GFA) is a measure of the easiness to vitrify a given substance. Theoretically, it is possible to make a glass from any liquid provided it is quenched from its *liquidus* temperature with a cooling rate above a critical value R_c to avoid crystallization. However, measuring GFA is a laborious and time-consuming task. Moreover, predicting the GFA of substances that have never been vitrified is of greater interest. Here, we propose and evaluate a new parameter that can predict the glass forming ability of oxide mixtures. We derived a mother parameter, $\mathrm{GFA} = 1/R_c \propto [U(T_{max}) \times T_L]^{-1}$, where $U(T_{max})$ is the maximum crystal growth rate, and T_L is the *liquidus* temperature, which strongly correlates with the experimental critical cooling rates of oxide glass-formers. A simplified version derived from the mother parameter—which does not need (scarce) crystal growth rate data and only relies on viscosity η and T_L, $\mathrm{GFA} \propto [\eta(T_L)/T_L^2]$—also correlates well with the R_c of several oxide compositions. This new GFA parameter, dubbed *Jezica*, works when heterogeneous nucleation prevails. It corroborates the widespread concept that substances having high viscosity at T_L, and a low T_L can be easily vitrified, and provides a powerful tool for the quest and design of novel glasses.

KEYWORDS

critical cooling rate, crystal growth, glass-forming ability, oxide glasses, viscosity

1 | INTRODUCTION

Glass has played a fundamental role in humankind well-being. During and after the scientific revolution of the XVII century, glasses were essential for the development of the thermometer, barometer, microscope, telescope, and many other useful devices, deservedly obtaining the status of "*the eyes of science*".[1] In recent years, improvement and discovery of novel inorganic glasses with a relevant combination of properties enabled a wide range of domestic and high-tech applications. For instance, glass windows have been greatly improved to provide greater comfort by reflecting or absorbing specific light wavelengths, by the ability to self-clean, and by displaying electrochromic properties.[2,3] Bioactive glasses and glass-ceramics can be used in ophthalmic cavity prostheses, ear bones, bone grafts, dental treatment, or healing of soft and hard tissues.[4] They are also used to immobilize nuclear waste, in hard disc substrates and as precursors of glass-ceramics used for ballistic protection.[5–8] Furthermore, in recent years, an impressive number of chalcogenide, organic, and metallic glasses have been developed, which have unusual, interesting properties.[9–14]

The vast number of applications of vitreous materials is due to the possibility of continuously adjusting their compositions to achieve optimum performance. Glasses are nonequilibrium, noncrystalline substances that spontaneously relax toward the supercooled liquid state,[15] with no constraint of satisfying crystal chemistry (stoichiometry) requirements.[16] This feature enables them to host practically any chemical element in the composition in widely variable amounts,

therefore a virtually infinite number of compositions can be explored.[17]

However, a liquid substance will only form a glass if nature can be tricked into (temporarily) freezing a disordered atomic structure before it assembles itself into a spatially periodic crystalline arrangement—which is the thermodynamically favorable state below the melting point, T_m, or *liquidus* temperature, T_L. Glass-forming ability (GFA) is a measure of the easiness to vitrify a liquid on cooling from its *liquidus* temperature.[18] Theoretically, any liquid can be vitrified as long as a quenching rate higher than a certain critical value (R_c) is imposed to avoid crystallization,[19] thus GFA = $1/R_c$. The R_c can be determined by cooling the liquid at different speeds, and then measuring the critical cooling rate to form only a small arbitrary crystallized fraction on the cooling path. These methods, however, are highly affected by the surface in contact with the supercooled liquid during the cooling, and the R_c determined by different authors can differ by orders of magnitude.[20–25] One can also determine the crystal nucleation and growth rates as a function of temperature, and then construct time-temperature-transformation (TTT), or continuous cooling transformation (CCT) curves[26,27] from which R_c can be calculated. The drawback is that constructing these curves is very time consuming.

Given the laborious task of obtaining R_c, some authors have suggested simpler, indirect parameters to estimate the GFA. Some are based on characteristic temperatures determined by thermal analysis, such as the glass transition, T_g, the onset of crystallization, T_x, and the *liquidus* temperature, T_L.[28–31] Moreover, a positive correlation between some of these parameters and the GFA of oxide glasses was indeed reported.[32,33] However, due to the lack of critical cooling rate data, just a few glass-forming substances were considered in those tests. In addition, to use these parameters one has to make a glass, which can then be scrutinized by differential thermal analysis (DTA) or differential scanning calorimetry (DSC). Hence, they only work for materials that can be vitrified, hence cannot be employed as predictors of GFA.

Within the recent data-driven modeling paradigm of materials development, a long-standing problem is to understand how the GFA correlates with properties that can be more easily measured or calculated from the chemical composition. It is thus highly desirable to predict (rather than measure) the GFA for the quest and design of novel vitrificable compositions.[34–36] Therefore, the aim of this work is to develop and test a new parameter that can predict the GFA.

2 | GOVERNING EQUATIONS

The R_c can be estimated by different methods. They are detailed below:

1. By computing CCT or isothermal TTT curves[26,27] that are calculated from available crystal nucleation and growth rates. This method is accurate but very time-consuming. It will be described in Section 2.1 and used here to derive a GFA parameter;
2. By analyzing the crystallization peak observed during the cooling of liquids in a differential thermal analysis equipment[37] or by combined cooling and heating experiments.[38,39] One issue of this technique is that it is highly susceptible to heterogeneous nucleation due to the contact of the liquid with the DTA pan[40];
3. By cooling the liquid at different rates and carrying out a microscopic or X-ray diffraction (XRD) analysis to determine if the sample is crystallized. The cooling process can be made by the "thermocouple method",[20–25] where the material remains in direct contact with a thermocouple, which gives a high accuracy in the temperature determination; in thermal analysis equipment[38,41]; or in the crucible where the material was melted. However, the thermocouple and the crucible material frequently induce heterogeneous nucleation, which affects the method's reproducibility. The reported values of these direct measures of R_c of melts having nominally the same composition reported frequently vary by one or two orders of magnitude.[20,25] Therefore, it should be stressed from the beginning that the errors in the values of R_c are always quite high.

2.1 | The TTT method

As stated before, one way to estimate the critical cooling rate of a substance is via its TTT diagram. One can use the Johnson-Mehl-Avrami-Kolmogorov (JMAK) equation[42] to build transformation curves as a TTT diagram. To do so, it is necessary to specify the desired crystallized volumetric fraction, X_V, and compute the time, t, to crystallize that fraction of the substance. For instance, considering homogeneous internal nucleation of tridimensional crystals, with time-independent crystal nucleation and growth rates, and a small volume fraction crystallized, X_V (typically in the range 10^{-2}-10^{-6}), the JMAK equation simplifies to

$$X_V = g_v I U^3 t^4, \tag{1}$$

where g_v is a shape factor related to the crystal morphology, I is the steady-state homogeneous crystal nucleation rate, and U is the crystal growth rate.

Most oxide supercooled liquids undergo heterogeneous surface nucleation and crystallization[43] due to the presence of foreign, spurious nucleation sites. In this case, the surface crystallized fraction, X_S, can be calculated by Equation 2,[44]

$$X_S = g N_S U^2 t^2, \tag{2}$$

where g is a factor related to the bi-dimensional shape of the crystals on the glass surface, and N_S is the average number of nucleation sites per unit area.

Figure 1 shows schematic TTT curves computed using Equations 1 and 2. In these curves, X_V, X_S, N_S, g_v, and g are constant. The critical cooling rate is thus the minimum rate needed to bypass a certain critical crystallized volume or surface fraction. It can be estimated from TTT diagrams by Equation 3.[26]

$$R_c \sim \frac{T_L - T_n}{t_n} \tag{3}$$

In Equation 3, T_n is the nose temperature, t_n is the time to crystallize a certain minimum fraction (usually taken as 10^{-2}-10^{-6}) at the nose temperature, and T_L is the melting point for stoichiometric compounds or the *liquidus* temperature for nonstoichiometric. T_L is the highest temperature where a crystalline phase is still stable; we will call this temperature the *liquidus* for simplicity from now on.

During casting and cooling, most supercooled liquids will likely be in contact with some solid particles or surface, which may induce heterogeneous (surface) nucleation. Moreover, the majority of oxide supercooled glass-forming liquids do not show any measurable homogeneous (internal) crystal nucleation. Therefore, it is reasonable to assume that, in most practical cases, the critical cooling rate is determined by heterogeneous nucleation. It is important to stress, however, for certain glass formers, the internal, homogeneous nucleation rates can be quite high, hence these assumptions may not hold. The surface crystallized fraction depends strongly on the number of nucleation sites, N_s, which in turn depends upon numerous factors.[43] The other two parameters in Equation 2, shape factor and crystal growth rate, depend only on the glass composition and temperature.

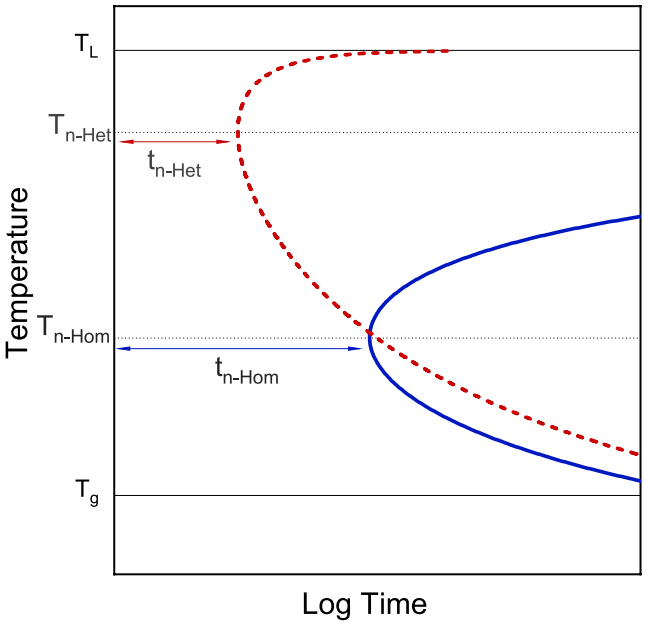

FIGURE 1 Schematics of TTT or "nose" curves: The continuous line refers to homogeneous nucleation, whereas the dashed line considers heterogeneous nucleation. T_L, T_n and T_g are the *liquidus*, the nose, and the glass transition temperature, respectively

2.2 | Classical crystal growth models for inorganic glasses

Three classical crystal growth models[45] describe the growth rate curves of inorganic glass-formers: the Normal or continuous growth (N), the Screw Dislocation growth (SD), and the 2D-secondary surface nucleation growth (2D). The SD growth model describes crystal growth in most inorganic glass forming substances. In this model, the crystal growth rates, U, are given by

$$U(T) = f(T)\frac{D_U(T)}{\lambda(T)}\left[1 - \exp\left(\frac{\Delta G(T)}{RT}\right)\right], \tag{4}$$

where f is the fraction of sites at the crystal interface available for atomic or molecular attachment, D_U is the effective atomic transport coefficient controlling crystal growth, λ is the jump distance, $\Delta G(T)$ is the free energy change in the transformation of the supercooled liquid to crystal (which is negative for spontaneous processes), R is the gas constant, and T is the absolute temperature.[46] In the N growth model, the crystal surface is considered to be rough on an atomic scale, hence there are plenty of sites for attachment of structural units and the parameter f is temperature independent and close to unity.

The 2D Secondary Nucleation growth model—Equation 5—relies on other parameters, C and B, which are related to the nucleation rate of the secondary nuclei that form in an atomically flat solid-liquid interface. For this model, the growth rates are given by

$$U(T) = \frac{C(T)D_U(T)}{\lambda^2(T)}\exp\left(\frac{B(T)}{RT}\right). \tag{5}$$

C and B can be calculated by different expressions depending upon the ratio of the secondary crystal nucleation rate to the crystal growth rate.[47] The B parameter includes the $\Delta G(T)$ and the energy of the crystal-liquid interface (σ^2), which can assume significantly different values for each glass-forming substance. Because of this fact, and the exponential dependency of U to σ^2, the 2D growth model does not have a reliable predictive power.

Several works[44,48] successfully connected D_U with the shear viscosity of the supercooled liquid using the Stokes-Einstein-Eyring equation,[49] but this connection breaks down for temperatures below 1.1-1.2T_g.[44,50–52] Fortunately, however, this break is not relevant for this particular work because we

will be dealing with crystallization at much higher temperatures, near to the nose of the TTT curves, which are close to T_L.

3 | NEW GFA PARAMETERS THAT CORRELATE WITH CRITICAL COOLING RATES

Equation 2 shows that on a TTT curve, the time needed to reach a certain surface crystallized fraction at each temperature is given by

$$t = \sqrt{\frac{X_s}{gN_S U^2}} \tag{6}$$

Here, we assume that the unknown fraction of heterogeneous surface sites, N_S, have a small variation between different liquids close to the *liquidus* temperature because the liquid surfaces are smooth, "fire-polished"-like. This is relevant because the nose of the heterogeneous TTT curve is located just below T_L (Figure 1). Thus, for the purpose of estimating R_c for different liquids, we assume that N_S is constant.

With the above considerations, the maximum time a melt can be considered noncrystalline at a temperature just below the *liquidus* temperature is inversely proportional to the crystal growth rate, $t(T) \propto \frac{1}{U(T)}$. The nose temperature, T_n, for heterogeneous nucleation is located at a temperature where the crystal growth rate is maximum, that is $T_n = T_{max}$, with $U(T_{max}) \equiv \max(U(T))$. Therefore, the nose time is given by Equation 7.

$$t_n \propto \frac{1}{U\left(T_{max}\right)} \tag{7}$$

Figure 2 shows experimental values of crystal growth rates for 20 stoichiometric oxide glass formers. T_{max} lies within the range of 0.90-0.98T_L for all the materials investigated, whereas the maximum crystal growth rate, $U(T_{max})$, varies seven orders of magnitude. A similar behavior of growth rates can be observed in relation to the *liquidus* temperature, T_L, for nonstoichiometric glasses (Table S1). For the sake of simplicity, from now on, we will use the average value, $T_{max} = 0.94T_L$.

With the previous considerations and Equation 3, an expression for R_c is given by Equation 8. This relatively simple new parameter, called herein "the mother parameter", will be tested in this article.

$$R_c = \frac{1}{GFA} \propto T_L U\left(T_{max}\right) \tag{8}$$

Unfortunately, experimental crystal growth rates are only available for a restricted number of substances. We then wondered if this parameter (Equation 8) could be simplified using

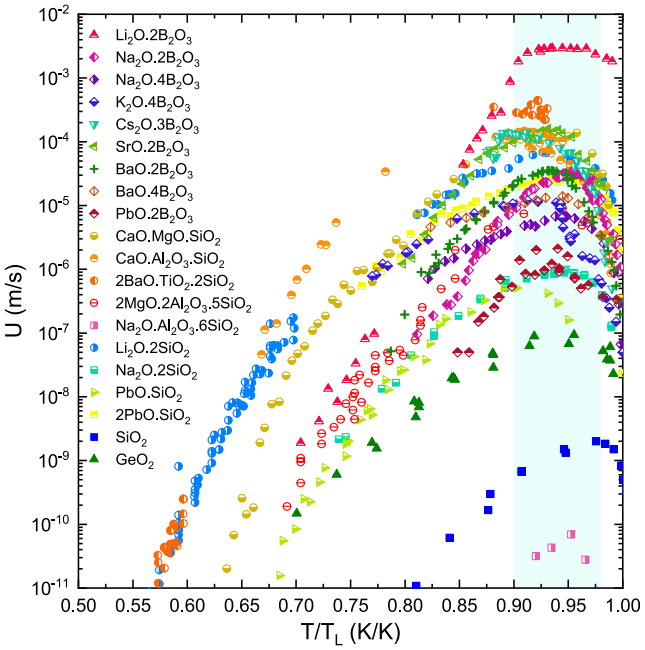

FIGURE 2 Crystal growth rate *vs*. reduced temperature for 20 stoichiometric oxide glass formers. We corrected the reported temperatures with the Herron and Bergeron (H-B) equation.[53] $U(T_{max})$ always occurs at a temperature between 0.90-0.98T_L (highlighted region)[54–72]

physical quantities that are more readily available. Therefore, we considered the most usual crystal growth model (the SD model) and assumed that the atomic transport coefficient, D_U, is controlled by the viscosity according to the well-known Stokes-Einstein-Eyring expression, Equation 9. In doing so, an expression for the maximum crystal growth rate shown in Equation 10 was obtained.

$$D_U(T) = D_\eta(T) = \frac{kT}{\eta(T)\,\lambda(T)} \tag{9}$$

$$\begin{aligned} U\left(T_{max}\right) &\approx U\left(0.94T_L\right) \\ &= f\frac{k_b 0.94T_L}{\lambda^2 \eta\left(0.94T_L\right)}\left[1-\exp\left(\frac{\Delta G}{R0.94T_L}\right)\right] \end{aligned} \tag{10}$$

After further investigation, we observed that the maximum variation of the thermodynamic factor $[1 - \exp(\Delta G(T)/RT_{max})]$, with $\Delta G < 0$, is only one order of magnitude for the 20 stoichiometric substances studied here. In addition, we expect that f is similar for all glass-forming oxide liquids at such low supercooling. With these considerations, we conclude that, for supercooled liquids that obey the SD model, the maximum growth rates, $U(T_{max})$, depend mostly on the shear viscosity, η.

Therefore, with Equation 8 and the arguments of the previous paragraph, for the SD growth model, the GFA (the inverse of the critical cooling rate) can be estimated by the following:

$$\mathrm{GFA} \propto \frac{\eta\left(0.94T_L\right)}{T_L^2}. \quad (11)$$

Because the shear viscosity usually varies little with temperature near the *liquidus* (the viscosity-temperature curve is flat in that region), $\eta(0.94T_L) \approx \eta(T_L)$, which leads to the final, simplified form of the GFA parameter:

$$\mathrm{GFA} \propto \frac{\eta(T_L)}{T_L^2}. \quad (12)$$

We baptized this simplified parameter "*Jezica*", which is easy to memorize. It stands for JZCA (Jiusti-Zanotto-Cassar-Andreeta,). *Jezica* has some appealing properties that will be discussed after testing it.

In this manuscript, we will thoroughly test the proposed mother parameter (Equation 8) and the simplified parameters (Equations 11 and 12), which are more easily assessable but, in principle, have a lower predicting power than Equation 8. For this test, we will use several stoichiometric and non-stoichiometric glass-forming compositions, covering a very wide range of glass-forming abilities, from outstanding to very poor.

4 | METHODS

4.1 | Data collection

We investigated 20 stoichiometric and 13 nonstoichiometric glass-forming oxides for which the maximum crystal growth rates and viscosities at the relevant temperatures (close to T_L) are known. We also used other 35 glasses for which the R_c have been measured.

As this work deals with numerous data from various sources, we tabulated all of them in Supporting information; in the manuscript, we only show the results in graphical form.

The dataset for the stoichiometric glasses is shown in Tables S2 and S3. This group includes two single oxide glasses, binary and ternary silicates, and binary borates. Among these, only the $Li_2O{\cdot}2SiO_2$, $Li_2O{\cdot}2B_2O_3$, $2BaO{\cdot}TiO_2{\cdot}2SiO_2$, and $CaO{\cdot}Al_2O_3{\cdot}SiO_2$ have been reported to show internal (homogeneous) nucleation when properly heated to temperatures in the range of 0.5-0.6T_L. However, internal nucleation is negligible for all studied compositions in the range of interest in this study (0.90-0.98T_L). The dataset for the nonstoichiometric glasses was collected from references [73,74] and includes 13 compositions that contain up to 10 different oxides (Table S1). Those glasses have commercial applications and are very good glass formers. The experimental R_c data used to test the mother parameter was collected from references [20,25]. These data are also shown in the final plot (see Tables S4 and S5).

4.2 | Homogeneous vs heterogeneous nucleation

In the derivation of the new parameters, we assumed that heterogeneous surface nucleation (which is, by far, the most common crystallization mechanism for oxide glasses) yields a higher value of R_c than homogeneous nucleation, thus heterogeneous nucleation controls GFA. However, we know a few inorganic glasses that also show copious (very high) internal homogeneous nucleation rates. To analyze the implications of the aforementioned assumption, we constructed TTT-diagrams considering homogeneous and heterogeneous nucleation for two stoichiometric compositions for which the internal (homogeneous) nucleation rates differ by 15 orders of magnitude: anorthite and fresnoite.

For the TTT-diagrams calculated considering heterogeneous nucleation, we assumed two different nucleation site densities: 10^5 and 10^1 sites per square meter. These site densities are typical for fractured and polished glass surfaces.[43] We used π as the characteristic crystal shape factor for all substances, since this parameter does not significantly affect the calculated critical cooling rates. We also assumed the same crystallized fraction for the homo and heterogeneous nucleation scenarios. Finally, to construct the TTT-curves we used Equations 1 and 2 with published data on crystal nucleation and growth rates. Then, the critical cooling rates for the anorthite and fresnoite glasses were calculated using Equation 3.

4.3 | Computing the critical cooling rates

Due to the scarcity of experimental R_c data, we calculated the critical cooling rates considering heterogeneous surface nucleation to test the validity of the proposed parameters. For this calculation, we considered an average of $N_S = 10^3$ sites/m^2 and $X_S = 10^{-2}$. The nose temperature was taken as the temperature of maximum growth rate, T_{max}, after applying the H-B correction[53] for the increased temperature—due to liberation of latent heat—at the growth front. However, for the nonstoichiometric glasses we used the reported T_{max} without the H-B correction, as the lack data on the entropy of fusion impedes the calculation. Luckily, however, as these growth rates are small, the correction would not be greater than 2 K. We then assumed a N distribution for each variable (excluding X_S), considering a standard deviation of 2% around the reported values of T_{max}, $U(T_{max})$, T_L, and a standard deviation of ± 1 in $\log(N_S)$. We used these distributions to draw a value for each variable, generating a dataset that we used to compute the R_c. Each new dataset had its own value of R_c. We repeated this numerical procedure 100 000 times to obtain a distribution of critical cooling rates for each glass. We then used the median of this distribution, and the values at 5th and 95th percentile as the bottom and upper limits of R_c in the plots. This procedure

was chosen to evaluate the uncertainty in R_c. This analysis was necessary to calculate with confidence the error propagation in this complex problem, for which the use of a simple error propagation method would not suffice.

4.4 | Calculating the parameters based on viscosity

We used a similar approach as presented in the previous Subsection to calculate the parameters proposed in Equations 11 and 12 with the respective uncertainty. Each drawn dataset contained a value of T_L, with this value and the VFT (Vogel-Fulcher-Tammann) equations[75–77] for each glass, we computed the values of $\eta(0.94T_L)/T_L^2$ and $\eta(T_L)/T_L^2$ (*Jezica*). By doing this for all the 100 000 generated datasets, we obtained a distribution of the parameters. The median and the values at 5th and 95th percentile of this distribution were used as the central, bottom and the upper limit in the plot, respectively.

4.5 | Statistical analysis

To verify the validity of the mother parameter (Equation 8), we used a statistical hypothesis test to evaluate if the logarithm of the experimental critical cooling rate and the logarithm of this first proposed parameter were linearly correlated.

Regarding the derived daughter parameters (Equations 11 and 12), we used two statistical hypothesis tests: one to check if there is a monotonic relation between these parameters and the calculated critical cooling rates; and other to check if there is a linear correlation between the logarithm of the parameters and the logarithm of the critical cooling rate. The first was done by computing the Spearman coefficient between the parameters and R_c for each generated dataset in Section 4.2. The second was done by computing the Pearson correlation coefficient between the logarithm of the parameters and the logarithm of R_c for each generate dataset in Section 4.2. In doing so, we obtained a distribution of the Spearman and Pearson coefficient.

All tests were conducted with a significance level of 95%, which means that we cannot reject the alternate hypothesis (linear correlation between the variables) if the *P*-value of the test is less than 0.05.

5 | RESULTS AND DISCUSSION

5.1 | TTT curves for homogeneous and heterogeneous nucleation

Figure 3 shows the TTT-curves of two glass-forming melts whose internal (homogeneous) nucleation rates differ by 15 orders of magnitude. Anorthite glass shows a maximum nucleation rate of approximately 10^2 m^{-3} s^{-1}, whereas fresnoite has a maximum of 10^{17} m^{-3} s^{-1}. Even for a small density of surface nucleation sites, the nose of the TTT curves for heterogeneous surface nucleation leads to shorter times compared to the nose of the homogeneous nucleation TTT curves. The equivalent N_S for a heterogeneous TTT curve to exhibit the same R_c as the homogeneous case would be around 10^{-2} and 10^{-1} sites per m^2 for anorthite and fresnoite glasses, respectively.

This difference between the two nucleation cases is because heterogeneous nucleation takes place on pre-existing active sites that are available for crystal growth at all temperatures below T_L, including T_{max} where the crystal growth rates are the highest. This analysis reinforces our approach of using a heterogeneous TTT-curve to determine the critical cooling

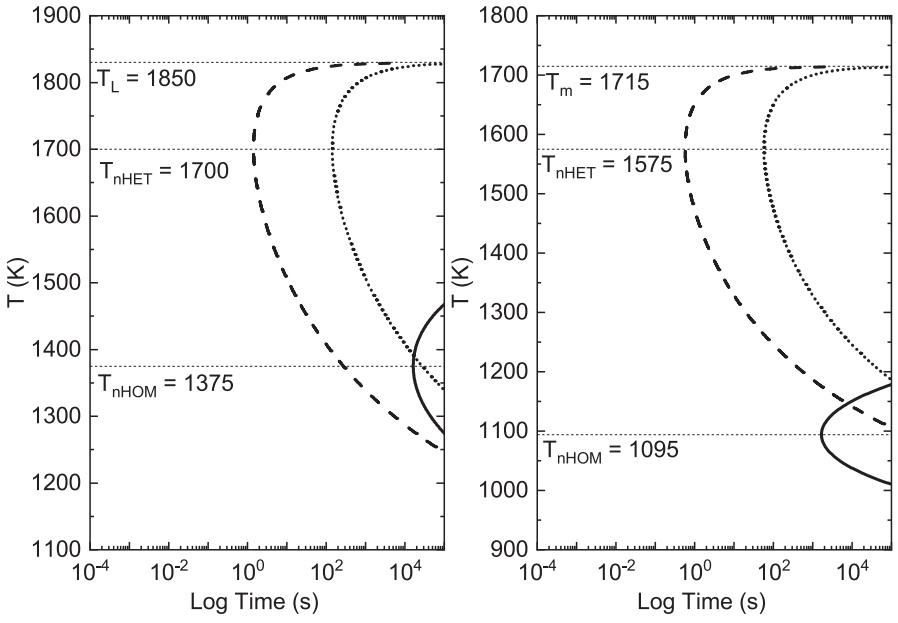

FIGURE 3 Temperature vs time in log scale: TTT curves for anorthite ($CaO{\cdot}Al_2O_3{\cdot}2SiO_2$) (left), and fresnoite ($2BaO{\cdot}TiO_2{\cdot}2SiO_2$) (right) considering X_S and $X_V = 10^{-2}$. Homogeneous nucleation (—). Heterogeneous surface nucleation for (- - -) $N_S = 10^5$ and (·····) $N_S = 10^1$. Although the nose times seem to be close to each other, we stress that the time scale is logarithmic

rates of oxide glasses because: (a) it is well-known that most glass-formers do not show measurable homogeneous nucleation; (b) even for fresnoite, the oxide glass-former showing the highest homogeneous nucleation rates known, heterogeneous nucleation seem to dominate the R_c. However, we emphasize that this scenario could change for materials having extremely high homogeneous nucleation rates, such as LJ (Lennard-Jones) liquids, pure metals, water, ionic liquids, and some metallic alloys ($I(T_{max}) \sim 10^{30}$ m^{-3} s^{-1})[78].

5.2 | Testing the mother parameter, GFA $\propto [U(T_{max})\cdot T_L]^{-1}$

Figure 4 shows a test of Equation 8, that is, the parameter $[U(T_{max})\cdot T_L]$ vs measured critical cooling rates. All seven data points[20,25] refer to binary silicate glasses, where LS_2, NS_2 and KS_2 are stoichiometric, and LS_3 and NS_3 are non-stoichiometric. One can see that the R_c reported by different authors differ considerably. The R_c of the NS_2 glass, for example, differs more than one order of magnitude, showing evidence of the difficulties in measuring this property. In any case, these data are very useful to illustrate the typical uncertainties.

Despite the scarcity of experimental data for R_c, Figure 4 indicates a linear correlation between R_c and the $[U(T_{max})\cdot T_L]$ parameter. To confirm our assumption, a linear regression with a unity slope would have to adjust the data points. The small P-value of 4 x 10^{-3} indeed indicates that we cannot reject the assumption that R_c is proportional to $[U(T_{max})\cdot T_L]$, with good statistical confidence. The intercept of the trend line is -1.6 ± 0.1, which relates to an average density of surface sites of 10^0-10^3 per m^2 for X_S of 10^{-6}-10^{-2} (Equations 3 and 6). This value of N_S indeed refers to the density of sites reported for fractured or polished surfaces.[43]

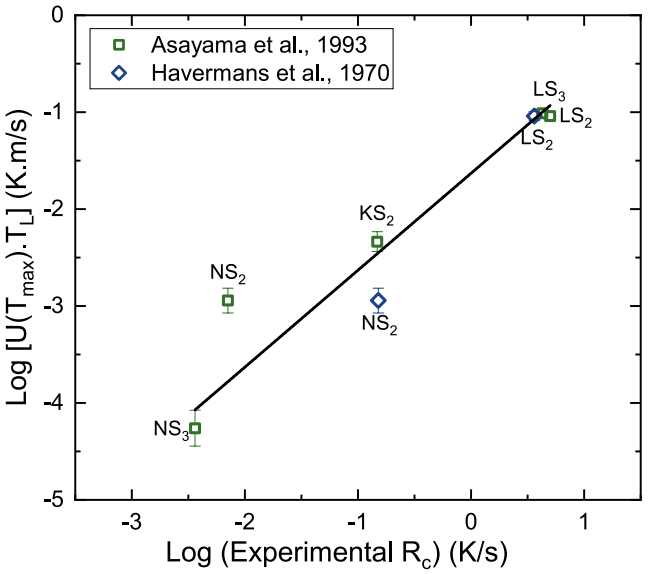

FIGURE 4 The mother parameter $[U(T_{max})\cdot T_L]$ vs critical cooling rates, R_c, determined by the continuous cooling method. Experimental R_c data for LS_2: $Li_2O{\cdot}2SiO_2$, LS_3: $Li_2O{\cdot}3SiO_2$, NS_2: $Na_2O{\cdot}2SiO_2$, NS_3: $Na_2O{\cdot}3SiO_2$, KS_2: $K_2O{\cdot}2SiO_2$. The vertical error bars were calculated with the following typical errors: 5K in T_L and 10% in $U(T_{max})$. The errors in the experimental R_c (horizontal axis) were not informed in the literature, however they can easily reach 1 o.m., as shown for NS_2

5.3 | Discussion about the growth models and $\eta\left(0.94T_L\right)/T_L^2$

Due to the lack of experimental values for the maximum growth rates ($U(T_{max})$) for most glasses, we used the SD crystal growth model to derive the parameter $\eta\left(0.94T_L\right)/T_L^2$ to infer GFA. Here, we analyze how sensitive our calculations are to the specific crystal growth mechanism controlling crystallization in each glass. In Figure 5, we analyze the $\eta\left(0.94T_L\right)/T_L^2$ parameter for stoichiometric glasses for which enough crystal growth rate data are available to enable inferences about the effect of the crystal growth model. The growth models assigned to each glass are identified in the plot. We emphasize that it is difficult to distinguish between the 2D and SD mechanisms because, in many situations, both models fit the experimental growth rate data reasonably well. The data points identified with the SD mechanism in Figure 5 were assigned to this model because they showed a somewhat better fit, but these results are still up for debate.[50,62,71]

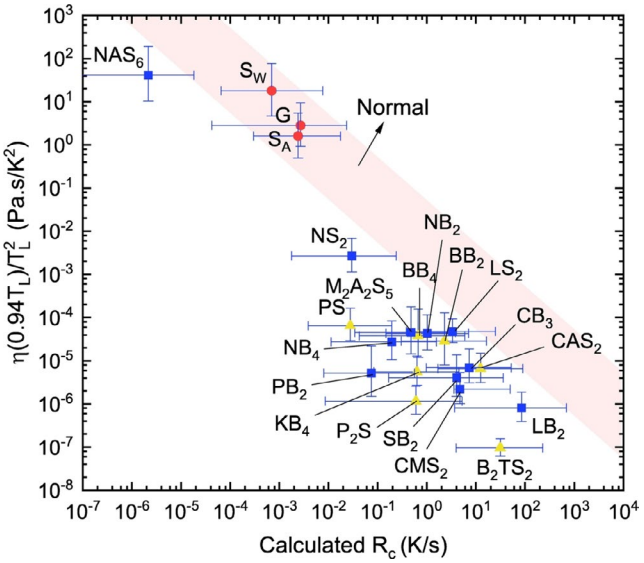

FIGURE 5 $\eta\left(0.94T_L\right)/T_L^2$ vs R_c calculated by the TTT nose method considering heterogeneous surface nucleation with $X_S = 10^{-2}$, $N_S = 10^3$ and corrected $U(T_{max})$ temperature. The range indicates the predicted region for glasses showing the N growth mechanism. Round points: N growth; square points: SD growth; triangular points: data best fit with the 2D model

For the N growth to prevail, the entropy of fusion must be inferior to $2R$ ($\Delta S_m < 2R$),[79] therefore, in our study, this mechanism only dominates for SiO_2 and GeO_2 glasses. The most frequent growth model, SD, differs from N growth only by the factor f, which is the fraction of sites available on the crystal surface for atomic attachment during crystal growth. At $0.94T_L$, $f \sim 10^{-2}$, meaning that $U(T_{max})$ is expected to be a hundred times smaller for glasses that have similar viscosity curves showing the SD growth mechanism compared to those that show N growth. On the other hand, substances that fit the N growth mechanism show a smaller entropy of fusion than those showing SD or 2D. Table S3 shows that the $1 - \exp(\Delta G/RT)$ factor for these two glasses is about one order of magnitude smaller than for the other glasses, which would lead to a lower R_c. If we consider only these two aspects, glasses showing the N growth mechanism should exhibit an R_c about one order of magnitude greater than those undergoing the SD growth mechanism. In the plot, glasses showing N growth are, in fact, in a region with higher critical cooling rates, but systems assigned to SD growth mechanism are distributed in a wider region, differing one or more orders of magnitude from the glasses showing N growth. This happens because we neglected the jump distance λ in our assumptions, and it can have different values for those glasses.

Regarding the 2D growth model, besides the influence of the jump distance, the calculated crystal growth rates can vary considerably between glass-forming melts due to the strong dependence on the crystal-melt interfacial energy. Within the glass-forming systems used in this work, literature results and our own analysis (not shown here) suggest that the growth rates of SB_2, BB_2, BB_4, LB_2, PS_2, PS, and B_2TS_2 could also fit the 2D model.[50,52,62,65,72] Figure 5 shows that the data referring to these glasses are also scattered over a relatively wide region. It is impossible, therefore, to assign a distinct region for SD and 2D models.

Furthermore, one should be aware that all these crystal growth models rely on several assumptions, including the hypothesis that only one mechanism dominates the growth rates in the entire temperature range. It is important to dwell on the specifics of the crystal growth models to understand the inaccuracy of the proposed parameter, which was predicted for the SD growth mechanism neglecting the effect of λ. However, as we will show in the next section, the relationship between GFA and the new parameter is quite reasonable for the experimental data explored here, regardless of the crystal growth mechanism that governs the process.

5.4 | Testing the *Jezica* parameter

Figure 6 shows a test of the *Jezica* parameter, Equation 12. The overall dataset includes 20 stoichiometric and 13 non-stoichiometric glasses. As a complementary test, we added 35

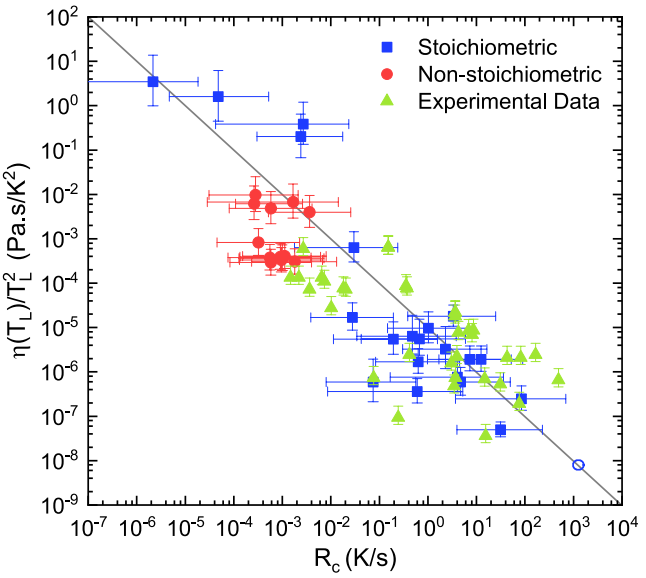

FIGURE 6 Test of the *Jezica*. $\eta(T_L)/T_L^2$ vs R_c in Log scale to cover 8 o.m. (■) Stoichiometric glasses and (●) Nonstoichiometric glasses, both with calculated R_c; (▲) Experimental R_c data; (○) Al_2O_3 = calculated *Jezica*. The continuous line represents the expected slope (−1) for the linear regression between $\log[\eta(T_L)/T_L^2]$ and $\log(R_c)$

glasses for which the R_c were experimentally determined (by different authors, using distinct methods) and the viscosities and *liquidus* temperatures are known. Finally, we also added an extremely poor oxide glass former, Al_2O_3, for which the viscosity and *liquidus* temperature are known.[80,81] The R_c for Al_2O_3 is not known for the conditions we considered ($N_S = 10^3$ and $X_S = 10^{-2}$), therefore we added the calculated *Jezica* value over the expected trend line. Since alumina is a pure oxide, the internal nucleation rates could be very high, hence the critical cooling rate is likely greater than the value predicted by the *Jezica* (that only takes surface crystallization into account). The Al_2O_3 datapoint was inserted just to give a reference of a possible lower limit for *Jezica*.

The data scatter is significant, however we have already shown that this wide variation is usual in R_c data, since the data originated from different laboratories, and they used different conditions to determine the R_c. The proposed parameter, however, indeed shows a clear visual correlation with the calculated R_c over a range of approximately 8 orders of magnitude. Besides, the experimental data agree reasonably well with the calculated set.

To evaluate if the relation between the variables is monotonic and also linear we used the (a) Spearman's coefficient and (b) Pearson coefficient, and two hypothesis tests, where the null hypotheses (H_0) were (a) inexistence of monotonicity and (b) inexistence of linearity. To reject H_0, the P-value must be less than 0.05. The monotonicity was evaluated between R_c and *Jezica* and the linearity was evaluated between the $\log(R_c)$ and $\log(Jezica)$ (Equation 12). Both analysis included

the 33 compositions which we were able to calculate R_c. If the predicted relation GFA $\propto 1/R_c$ is correct, the fitted slope in the linear regression should be −1. Figure 7 shows the frequency histograms of the Spearman's coefficient and *P*-value for the monotonicity test; the linear regression coefficient (Pearson's coefficient), the *P*-value for the linearity test and the slope of the linear regression.

The Spearman coefficient in Figure 7A shows a higher frequency around −0.80 and that the *P*-value (Figure 7B) for the monotonicity test is below 0.05, with higher frequency $P \sim 10^{-10}$, meaning we cannot reject the hypothesis of a monotonic relationship between the R_c and *Jezica*. These results endorse the existence of a relationship between these variables without applying the log scale.

Figures 7C-E show the histograms for the statistical parameters of linearity for the log(R_c) vs log(*Jezica*). The Pearson coefficient and the *P*-value show a distribution around −0.87 and $\sim 10^{-10}$, respectively, meaning that we cannot reject the assumption that the critical cooling rate is indeed correlated with the *Jezica* parameter. The slope of the linear regression is −0.92, which is close to the expected value of −1.00 with the assumptions made in Section 3. The analysis of the $\eta\left(0.94T_L\right)/T_L^2$ parameter (Figure S1) returned a similar correlation coefficient, with a slope of −0.95. Since the *Jezica* parameter is an approximation, it was indeed expected that the $\eta\left(0.94T_L\right)/T_L^2$ returned a slope closer to the predicted value.

In summary, the mother parameter (Equation 8), can be used to estimate the GFA if one can access $U(T_{max})$, because it has fewer assumptions than the derived parameters, Equations 11 and 12. However, if $U(T_{max})$ is not available—which is often the case—the $\eta\left(0.94T_L\right)/T_L^2$ parameter is slightly more precise, but our results show that the approximation $\eta\left(T_L\right)/T_L^2$ (*Jezica*) can be equally used with great advantage of being more easily determined, even for extremely reluctant glass-forming melts that cannot be cooled below T_L.

Figure 6 provides a tool to correlate the *Jezica* with the R_c, and to distinguish liquids of widely distinct vitrification ability, as shown in Table 1.

It is relevant to estimate the upper and lower limits of the *Jezica*. The maximum T_L reported is Hafnium Carbide's (HfC) = 4232 K.[82,83] If we consider a lower limit for the viscosity at T_L as 10^{-3} Pa s, then the lowest possible value of Log(*Jezica*) would be around −11. For an oxide, the maximum

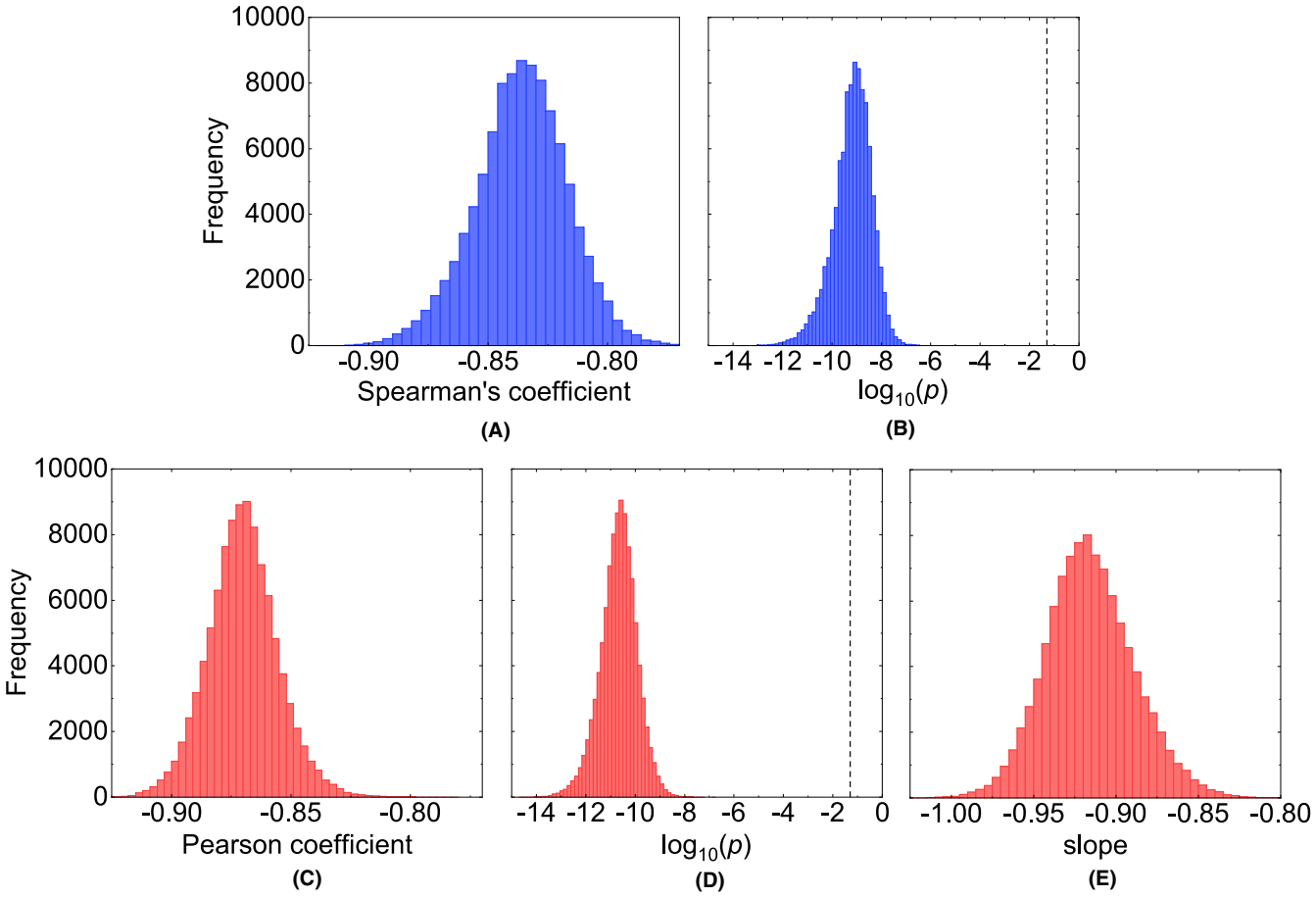

FIGURE 7 Frequency histograms of the: (A) Spearman coefficient and (B) *P*-value of the test of hypothesis of monotonicity; and (C) Pearson coefficient, (D) *P*-value of the test of hypothesis and (E) slope of the linear regression for the variables $x = \log(R_c)$ and $y = \log[\eta(T_L)/T_L^2]$

TABLE 1 R_c, Jezica and glass-forming classes

Log (R_c), (K/s)	Log [η (T_L)/T_L^2], Jezica, (Pa s/K^2)	Vitrification class
<−4	>−1	Outstanding
−4 to −1	−1 to −4	Good (commercial glasses)
−1 to 2	−4 to −7	Reluctant to poor
>2	<−7	Extremely poor

T_L is for ThO_2 = 3363 K, for which Log(*Jezica*) = −10. In fact, the region below the minimum value (−8) probed in this work includes substances that exhibit other crystal growth mechanisms; for example, the ultrafast crystal growth reported for some pure metals,[84] and also substances with extremely high internal nucleation rates, for which the *Jezica* may not work.

Regarding the upper bound, albite glass shows the highest value, Log(*Jezica*) is approximately 0.5, and is probably close to the maximum. Therefore, the *Jezica* spans about 12 orders of magnitude, from extremely good glass-formers to incredibly reluctant: +1 < Log(*Jezica*) < −11 (*Jezica* in SI units). In this article, we covered materials within the range +1 to −8.

The *Jezica* parameter is based only on a thermodynamic and a kinetic property, T_L and η, respectively, both of them implicitly carrying chemical and structural information of each material. This parameter bears a very important feature; it is not necessary to make a glass to measure the viscosity of the liquid and the respective *liquidus* temperature. *Jezica* corroborates the widespread empirical concept within the materials science community that substances having high viscosity at the *liquidus* and low *liquidus* (e.g., eutectics) can be easily vitrified. We hope that the success of this new parameter to describe the GFA of oxide compositions motivates further tests and research on the vitrification capacity of chalcogenide, metallic, and organic liquids to explore its possible generalization. Of special relevance would be the use of Machine Learning techniques[85] to predict the GFA of novel, yet unknown, materials using this parameter because both viscosity and *liquidus* temperatures are, in principle, calculable from the chemical composition.

6 | CONCLUSIONS

We derived and successfully tested new parameters that are able to predict the GFA of oxide liquids. The mother parameter, GFA $\propto [U(T_{max}) \times T_L]^{-1}$, strongly correlates with the experimentally determined critical cooling rates of oxide glass formers. However, (scarce) crystal growth rate data are necessary to use this parameter.

A simplified parameter that combines a kinetic and a thermodynamic property, GFA $\propto \eta(T_L)/T_L^2$, does not need crystal growth data and works equally well. It shows a robust correlation with the critical cooling rates of several oxide glass-formers spaning several orders of magnitude. This parameter was derived and works when heterogenous nucleation prevails over homogenous nucleation, which is often the case. It bears a very attractive feature; it is not necessary to make a glass to measure the viscosity of the liquid and the respective *liquidus* temperature. Finally, this new GFA predictor corroborates the widespread concept that substances having high viscosity at the liquidus and a low T_L are easily vitrified, providing a powerful predictive tool for the quest and design of novel oxide glasses.

ACKNOWLEDGMENTS

This study was financed in part by the Coordenação de Aperfeiçoamento de Pessoal de Nível Superior - Brasil (CAPES) - Finance Code 001, by the Conselho Nacional de Desenvolvimento Científico e Tecnológico (CNPq), grants #141107/2016-2 (JJ), and #300959/2010-9 (EDZ), and by the São Paulo Research Foundation (FAPESP) grants #2013/07793-6 (CEPID) and #2017/12491-0 (DRC).

ORCID

Jeanini Jiusti https://orcid.org/0000-0001-9923-2503
Edgar D. Zanotto https://orcid.org/0000-0003-4931-4505
Daniel R. Cassar https://orcid.org/0000-0001-6472-2780
Marcello R. B. Andreeta https://orcid.org/0000-0002-8436-5706

REFERENCES

1. Bolt M. Glass: the eye of science. Int J Appl Glas Sci. 2017;8(1):4–22.
2. Paz Y, Luo Z, Rabenberg L, Heller A. Photooxidative self-cleaning transparent titanium dioxide films on glass. J Mater Res. 1995;10(11):2842–8.
3. Mortimer RJ. Organic electrochromic materials. Electrochim Acta. 1999;44(18):2971–81.
4. Crovace MC, Souza MT, Chinaglia CR, Peitl O, Zanotto ED. Biosilicate®—a multipurpose, highly bioactive glass-ceramic. In vitro, in vivo and clinical trials. J Non Cryst Solids. 2016;432:90–110.
5. Ojovan MI, Batyukhnova OG. Glasses for nuclear waste immobilization. Paper presented at: WM Symposia, 2007. Proceedings of the 33rd annual waste management conference & exhibition; 2007 Feb 25 - Mar 01; Tucson (AZ) 2008. Curran Associates, Inc; p. 451-65.
6. Mccloy JS, Goel A. Glass-ceramics for nuclear-waste immobilization. MRS Bull. 2017;42(3):233–40.
7. Benitez T, Gómez SY, de Oliveira A, Travitzky N, Hotza D. Transparent ceramic and glass-ceramic materials for armor applications. Ceram Int. 2017;43(16):13031–46.

8. Eda S, Iono H, Maeda T, Tsuchiya H, Marumo Y. Glass substrate for a magnetic disk and magnetic disk. United States patent 8785010 B2. 2014 Jul 22. Hoya Corp, assignee.
9. Şopu D, Albe K, Eckert J. Metallic glass nanolaminates with shape memory alloys. Acta Mater. 2018;159:344–51.
10. Pan J, Wang YX, Li Y. Ductile fracture in notched bulk metallic glasses. Acta Mater. 2017;136:126–33.
11. Wegner G. Functional polymers. Acta Mater. 2000;48(1):253–62.
12. Srichana T, Domb AJ. Polymeric biomaterials. Biomed Mater. 2009;48:83–119.
13. Chen Y, Pan H, Mu S, Wang G, Wang R, Shen X, et al. Intermediate crystallization kinetics in germanium-tellurides. Acta Mater. 2019;164:473–80.
14. Dahshan A, Aly KA. Optical constants of new amorphous As-Ge-Se-Sb thin films. Acta Mater. 2008;56(17):4869–75.
15. Zanotto ED, Mauro JC. The glassy state of matter: its definition and ultimate fate. J Non Cryst Solids. 2017;471(May):490–5.
16. Mauro JC. Decoding the glass genome. Curr Opin Solid State Mater Sci. 2018;22(2):58–64.
17. Zanotto ED. A bright future for glass-ceramics. Am Ceram Soc Bull. 2010;89(8):19–27.
18. Weinberg MC. Glass-formation and crystallization kinetics. Thermochim Acta. 1996;280-281(SPEC. ISS.):63–71.
19. Kauzmann W. The nature of the glassy state and the behavior of liquids at low temperatures. Chem Rev. 1948;43(2):219–56.
20. Asayama E, Takebe H, Morinaga K. Critical cooling rates for the formation of glass for silicate melts. ISIJ Int. 1993;33(1):233–8.
21. Fang CY, Yinnon H, Uhlmann DR. A kinetic treatment of glass formation. VIII: critical cooling rates for Na_2OSiO_2 and K_2OSiO_2 glasses. J Non Cryst Solids. 1983;57(3):465–71.
22. Huang W, Ray CS, Day DE. Dependence of the critical cooling rate for lithium-silicate glass on nucleating agents. J Non Cryst Solids. 1986;86(1–2):204–12.
23. Lin B, Wang H, Zhu X, Liao Q, Ding B. Crystallization properties of molten blast furnace slag at different cooling rates. Appl Therm Eng. 2016;96:432–40.
24. Esfahani S, Barati M. Effect of slag composition on the crystallization of synthetic CaO-SiO_2-Al_2O_3-MgO slags: part I—crystallization behavior. J Non Cryst Solids. 2016;436:35–43.
25. Havermans A, Stein HN, Stevels JM. Critical cooling rates in alkali silicate systems. J Non Cryst Solids. 1970;5:66–9.
26. Weinberg MC, Zelinski BJ, Uhlmann DR, Zanotto ED. Critical cooling rate calculations for glass formation. J Non Cryst Solids. 1990;123(1–3):90–6.
27. Clavaguera N. Non-equilibrium crystallization, critical cooling rates and transformation diagrams. J Non Cryst Solids. 1993;162(1–2):40–50.
28. Lu ZP, Liu CT. A new glass-forming ability criterion for bulk metallic glasses. Acta Mater. 2002;50(13):3501–12.
29. Hrubý A. Evaluation of glass-forming tendency by means of DTA. Czechoslov J Phys. 1972;22(11):1187–93.
30. Long Z, Wei H, Ding Y, Zhang P, Xie G, Inoue A. A new criterion for predicting the glass-forming ability of bulk metallic glasses. J Alloys Compd. 2009;475(1–2):207–19.
31. Chattopadhyay C, Satish Idury K, Bhatt J, Mondal K, Murty BS. Critical evaluation of glass forming ability criteria. Mater Sci Technol. 2016;32(4):380–400.
32. Nascimento M, Souza LA, Ferreira EB, Zanotto ED. Can glass stability parameters infer glass forming ability? J Non Cryst Solids. 2005;351(40–42):3296–308.
33. Cabral AA, Cardoso A, Zanotto ED. Glass-forming ability versus stability of silicate glasses. I. Experimental test. J Non Cryst Solids. 2003;320(1–3):1–8.
34. Gross O, Riegler SS, Stolpe M, Bochtler B, Kuball A, Hechler S, et al. On the high glass-forming ability of Pt-Cu-Ni/Co-P-based liquids. Acta Mater. 2017;141:109–19.
35. Shamlaye KF, Laws KJ, Löffler JF. Exceptionally broad bulk metallic glass formation in the Mg-Cu-Yb system. Acta Mater. 2017;128:188–96.
36. Kuball A, Bochtler B, Gross O, Pacheco V, Stolpe M, Hechler S, et al. On the bulk glass formation in the ternary Pd-Ni-S system. Acta Mater. 2018;158:13–22.
37. Barandiarán JM, Colmenero J. Continuous cooling approximation for the formation of a glass. J Non Cryst Solids. 1981;46(3):277–87.
38. Ray CS, Reis ST, Brow RK, Höland W, Rheinberger V. A new DTA method for measuring critical cooling rate for glass formation. J Non Cryst Solids. 2005;351(16–17):1350–8.
39. Liu S, Tao H, Zhang Y, Yue Y. A new approach for determining the critical cooling rates of nucleation in glass-forming liquids. J Am Ceram Soc. 2017;100(9):3875–82.
40. Krüger S, Deubener J. Stochastic nature of the liquid-to-crystal heterogeneous nucleation of supercooled lithium disilicate liquid. J Non Cryst Solids. 2014;388:6–9.
41. Cabral AA, Fredericci C, Zanotto ED. A test of the Hrubÿ parameter to estimate glass-forming ability. J Non Cryst Solids. 1997;219:182–6.
42. Weinberg MC, Birnie DP, Shneidman VA. Crystallization kinetics and the JMAK equation. J Non Cryst Solids. 1997;219:89–99.
43. Müller R, Zanotto ED, Fokin VM. Surface crystallization of silicates glasses: nucleation and kinetics. J Non Cryst Solids. 2000;274:208–31.
44. Nascimento M, Dutra ZE. Does viscosity describe the kinetic barrier for crystal growth from the liquidus to the glass transition? J Chem Phys. 2010;133(17):174701.
45. Uhlmann DR. Crystal growth in glass-forming systems - A review. In: Hench LL; Freiman SW, editors. Advances in nucleation and-crystallization in glasses. Columbus, Ohio: American Ceramic Society, 1972. v. 5, p. 91–115.
46. Nascimento M, Ferreira EB, Zanotto ED. Kinetics and mechanisms of crystal growth and diffusion in a glass-forming liquid. J Chem Phys. 2004;121(18):8924–8.
47. Fokin VM, Yuritsyn NS, Zanotto ED. Nucleation and crystallization kinetics in silicate glasses: theory and experiment. In: Schmelzer J, editor. Nucleation Theory and Applications. Berlin/Weinheim, Germany: Wiley-VCH, 2005; p. 455.
48. Ediger MD, Harrowell P, Yu L. Crystal growth kinetics exhibit a fragility-dependent decoupling from viscosity. J Chem Phys. 2008;128(3):1–7.
49. Einstein A. On the movement of small particles suspended in stationary liquids required by the molecular-kinetic theory of heat. Ann Phys. 1905;17:549–60.
50. Nascimento M, Fokin VM, Zanotto ED, Abyzov AS. Dynamic processes in a silicate liquid from above melting to below the glass transition. J Chem Phys. 2011;135(19):1–17.
51. Cassar DR, Rodrigues AM, Nascimento M, Zanotto ED. The diffusion coefficient controlling crystal growth in a silicate glass-former. Int J Appl Glas Sci. 2018;9(3):373–82.
52. Cassar DR, Lancelotti RF, Nuernberg R, Nascimento M, Rodrigues AM, Diz LT, et al. Elemental and cooperative diffusion

in a liquid, supercooled liquid and glass resolved. J Chem Phys. 2017;147(1):014501.
53. Herron LW, Bergeron CG. Measurement of melt-crystal interface temperature during crystallisation in melts of binary borate glasses. Phys Chem Glas. 1978;19(5):89–94.
54. Vergano PJ, Uhlmann DR. Crystallisation kinetics of germanium dioxide: the effect of stoichiometry on kinetics. Phys Chem Glasses. 1970;11(2):30–8.
55. Wagstaff FE. Crystallization and melting kinetics of cristobalite. Am Ceram Soc. 1969;52(12):650–4.
56. Nascimento MLF. Problemas correntes sobre nucleação, crescimento de cristais e difusão em vidros. São Carlos (SP): Federal University of São Carlos, PhD thesis; 2004.
57. Nagel SR, Herron LW, Bergeron CG. Crystal growth of $Li_2B_4O_7$. J Am Ceram Soc. 1977;60:172–3.
58. Nagel SR, Bergeron CG. Crystallization of $Na_2B_4O_7$ from its melt. J Am Ceram Soc. 1974;57(3):129–31.
59. Leedecke CJ, Bergeron CG. Crystallisation of $Na_2B_8O_{13}$ in selected Na_2O-B_2O_3 melts. Phys Chem Glasses. 1977;18(6):166–220.
60. Leedecke CJ, Bergeron CG. The growth of $K_2B_8O_{13}$ in its stoichiometric melt. J Cryst Growth. 1976;32(3):327–31.
61. Marlor AJ, Kumar H, Bergeron CG. Crystallisation of caesium hexaborate from its undercooled melt. Phys Chem Glasses. 1975;16(5):108–11.
62. Bergeron CG. Crystal Growth Kinetics in Binary Borate Melts. In: Pye LD, Fréchette VD, Kreidl NJ editors. Borate Glasses. Materials Science Research, Boston: Springer, vol 12. 1978; p. 445–62.
63. Laird JA, Bergeron CG. Chain-folding mechanism for growth of $BaO_2B_2O_3$ crystal in its melt. J Am Ceram Soc. 1970;53:482–5.
64. Chialanza MR, Castiglioni J, Fornaro L. Crystallization as a way for inducting thermoluminescence in a lead borate glass. J Mater Sci. 2012;47(5):2339–44.
65. Rita RA, Bergeron CG. Crystallization of Pb_2SiO_4. J Am Ceram Soc. 1976;59:274–5.
66. Vakhrameev NA. Thermal effects at heating of glasses in the system Na_2O-PbO-SiO_2 (in Russian). In: Fiziko-Khimicheskie Svoistva Troinoi Sistemy Na_2O-PbO-SiO_2. 1949. p. 139–46.
67. Neiman T, Yinnon H, Uhlmann DR. Crystallization kinetics of lead metasilicate. J Non Cryst Solids. 1982;48:393–403.
68. Matusita K, Tashiro M. Rate of crystal growth in $Li_2O{\cdot}2SiO_2$ glass. J Ceram Assoc Japan. 1973;81:500–6.
69. Meiling GS. Crystallization Kinetics of Sodium Disilicate. Cambridge, MA: Massachusetts Institute of Technology. 1966.
70. Uhlmann DR, Yinnon H, Cranmer D. Crystallization behavior of albite. Lunar Planet Sci Conf. 1980;1178–80.
71. Reinsch S, Nascimento M, Müller R, Zanotto ED. Crystal growth kinetics in cordierite and diopside glasses in wide temperature ranges. J Non Cryst Solids. 2008;354:5386–94.
72. Kirkpatrick RJ, Robinson GR, Hays JF. Kinetics of crystal growth from silicate melts: anorthite and diopside. J Geophys Res. 1976;81:5715–20.
73. Brix P, inventor; Linz W. Aluminosilicate glass for flat display services. Europe patent 0879800A1, 1998 Nov 25. Schott AG, assignee.
74. Battigelli JA, inventor; Bouquet F. Glass composition and fibers. United States patent 4203774A, 1980 May 20. inventor; Massol J-J, inventor; Saint-Gobain Industries, assignee.
75. Vogel H. Das temperatureabhängigketsgesetz der viskosität von flüssigkei- ten. Phys Zeitschrift. 1921;22:645–6.
76. Fulcher GS. Analysis of recent measurements of the viscosity of glasses. J Am Ceram Soc. 1925;8(6):339–55.
77. Tammann G, Hesse W. Die Abhängigkeit der Viscosität von der Temperatur bie unterkühlten Flüssigkeiten. Zeitschrift für Anorg und Allg Chemie. 1926;156(1):245–57.
78. Tipeev AO, Zanotto ED, Diffusivity R. Interfacial free energy and crystal nucleation in a supercooled Lennard-Jones liquid. J Phys Chem C. 2018;122(60):28884-94.
79. Jackson KA. Current concepts in crystal growth from the melt. Prog Solid State Chem. 1967;4:53–6.
80. Hakamada S, Nakamura A, Watanabe M, Kargl F. Surface oscillation phenomena of eerodynamically levitated molten Al_2O_3. Int J Microgravity Sci Appl. 2017;34(4):340403.
81. Langstaff D, Gunn M, Greaves GN, Marsing A, Kargl F. Aerodynamic levitator furnace for measuring thermophysical properties of refractory liquids. Rev Sci Instrum. 2013;84(12):124901.
82. Toth LE. Transition Metal Carbides and Nitrides. New York, NY/London, UK: Academic Press; 1971: p. 279.
83. Cedillos-Barraza O, Manara D, Boboridis K, Watkins T, Grasso S, Jayaseelan DD, et al. Investigating the highest melting temperature materials: a laser melting study of the TaC-HfC system. Sci Rep. 2016;6(October):1–11.
84. Sun G, Xu J, Harrowell P. The mechanism of the ultrafast crystal growth of pure metals from their melts. Nat Mater. 2018;17(10):881–6.
85. Cassar DR, Carvalho ACPLF, Zanotto ED. Predicting glass transition temperatures using neural networks. Acta Mater. 2018;159:249–56.

SUPPORTING INFORMATION

Additional supporting information may be found online in the Supporting Information section at the end of the article.

How to cite this article: Jiusti J, Zanotto ED, Cassar DR, Andreeta MRB. Viscosity and liquidus-based predictor of glass-forming ability of oxide glasses. *J Am Ceram Soc*. 2019;00:1–12. https://doi.org/10.1111/jace.16732